Initial Results of a Multi-Constellation ARAIM Airborne Prototype

Juan Blanch, R. Eric Phelts, Yu-Hsuan Chen, Per Enge, *Stanford University*

ABSTRACT

Advanced Receiver Autonomous Integrity Monitoring extends RAIM to multiple constellations and dual frequency, with the goal of providing worldwide coverage of vertical guidance for aircraft. Availability simulations have shown that ARAIM based on GPS L1-L5 and Galileo E1-E1a could provide global coverage of vertical guidance. However these simulations rely on a set of assumptions on the measurements. In this paper we analyze a set GPS and Galileo measurements collected in flight. We characterize the multipath of different signal combinations and compare them to the models assumed in the ARAIM simulations. Using these models we apply the ARAIM airborne algorithm for set of constellation – signal configurations.

INTRODUCTION

Advanced Receiver Autonomous Integrity Monitoring (ARAIM) is a proposed concept that extends RAIM to multiple constellations and dual frequency, with the goal of providing worldwide coverage of vertical guidance for aircraft [7]. Availability simulations [7] have shown that ARAIM based on a nominal L1-l5 GPS-E1-E5a Galileo configuration (24 satellites each) would provide global coverage of LPV-200 [7]. These simulations rely on a set of assumptions on the new GNSS signals and the behavior of the airborne receiver. Among others, the availability results rely heavily on the following assumptions:

- when a satellite is above an elevation of 5 degrees, it will be tracked. It is known however that as the aircraft banks, there is the risk of losing track of low elevation satellites.
- the code noise and multipath is well bounded by the elevation dependent curve defined in [7], which is in turn an adaptation of the performance required in [6]. This curve is supposed to bound the code noise and multipath of the carrier-smoothed code.
- it can be assumed that cycle slips are rare enough, so that the error bound on the multipath is almost always the one provided by the bound on the carrier-smoothed code

Previous work has evaluated ARAIM in static receivers ([2], [3]), or using L1-L2 semi-codeless [1]. The main goal of this work is to evaluate how the assumptions listed above hold in an ARAIM airborne prototype using L1-L5 for GPS and E1-E5a for Galileo, which are signals for which ARAIM is designed (at least initially). We will also look at the performance of GLONASS, as it is, after GPS, the most complete constellation.

Set up and hardware

For this evaluation, we will use the data collected in the flight test campaign described in [1]. The receiver a (Trimble BX935-INS) tracked all the current GNSS constellations, satellites, and signals; in particular GPS, (L1 C/A, L1C, L2 (semi-codeless), L2C, and L5) and Galileo (E1 and E5a-E5b). This receiver was flown in a Global 5000 jet owned and operated by the William J. Hughes FAA Technical Center. The two three hour flights included straight and level phases, missed approaches, and “figure eights” (to evaluate the impact of banking).

In our analysis, we will address each of the three above assumptions: first, we will evaluate the noise of the carrier smoothed code and compare it against the assumed error bounds. Then, we will examine how aircraft banking affects

the reception of the GNSS signals. We will apply the ARAIM airborne algorithms ([4],[5]) to the L1-L5 GPS and E1-E5 Galileo signals to obtain the resulting ARAIM outputs (Vertical and Horizontal Protection Levels, Effective Monitor Threshold, and predicted accuracy). Finally, we evaluate how the pseudorange residuals compare to the assumed models, and the effect on the ARAIM test statistics.

MULTIPATH CHARACTERIZATION

In this section we compare the magnitude of the multipath to the error model assumed in [7]. This model, which only needs to apply after carrier smoothing for 100s, specifies an elevation dependent gaussian distribution. This model is adequate only if the corresponding gaussian distribution is an upper bound of the actual distribution. There are two related objectives in this section: verifying the bound for smoothing times larger than 100s and determining how to modify the formula for shorter smoothing times. This last point is important in this prototype because the large number of cycle slips prevents long smoothing times. We do stress that the results described here might be very dependent on the antenna installation, the receiver configuration, its performance, and that the amount of data is not sufficient to make any definitive claim. The Appendix includes analyses that, while not directly relevant to our prototype, could be useful in other applications. The analysis performed here only included data from one flight (August 25, 2016).

Carrier leveling

We estimated the multipath magnitude by performing carrier leveling on continuous arcs of more than 600 s (that is, intervals with no data gaps and no cycle slips). For each arc, we form the difference between code and phase for each frequency. For each pair of frequencies we also form the ionospheric free combination. Figure 2 and 3 show an example for GPS L1-L5. In Figure 2, the aircraft is not moving, which explains the long temporal correlation in the code multipath. We can also observe an instance of a relatively large multipath delay (which occurred when the aircraft was static).

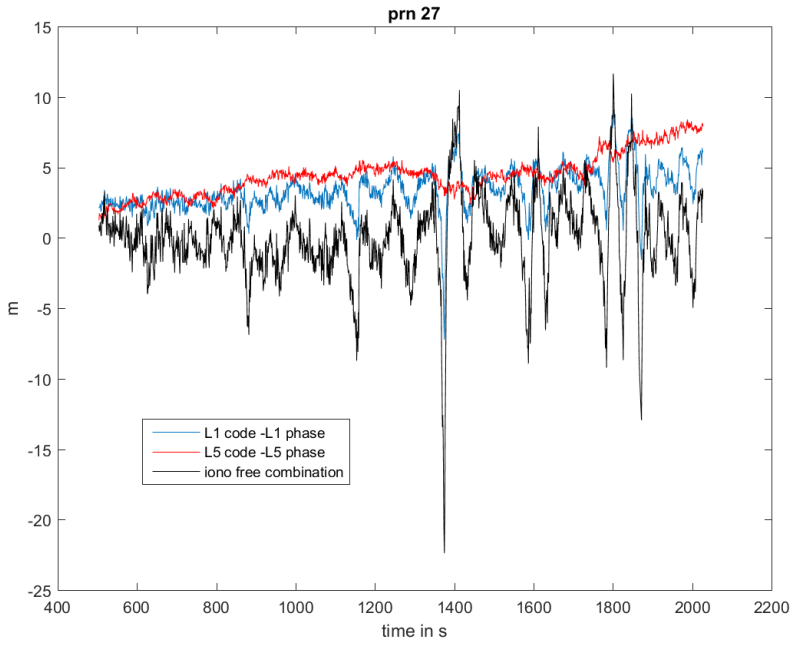

Figure 2. Code minus carrier combinations for GPS PRN 27.

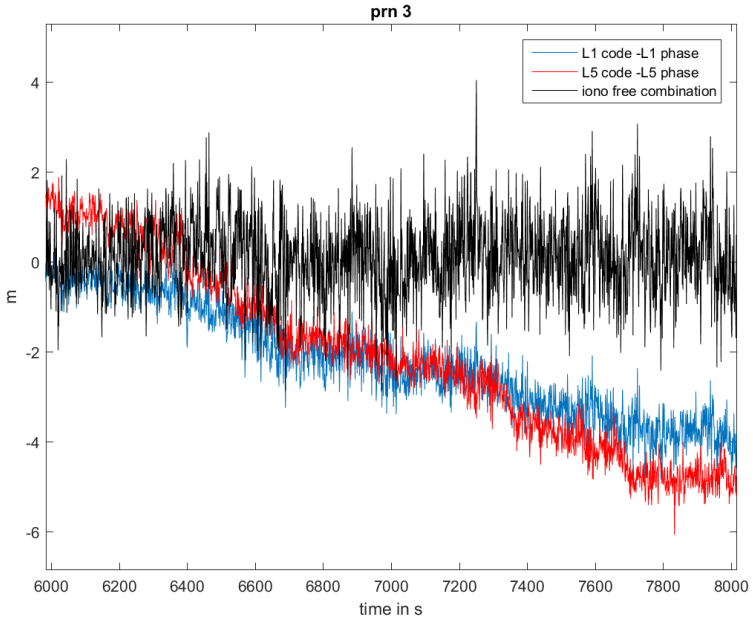

Figure 3. Code minus carrier combinations for GPS PRN 3.

The arc shown in Figure 3 corresponds to level flight, and the temporal correlation appears to be shorter. In both Figures, the trends in the single frequency combinations are due to the ionospheric delay. From now on, we will only study the dual frequency combinations. By assuming that the code multipath has a mean of zero over the arc, we can estimate the code multipath, as well as the carrier smoothed multipath. This provides an estimate $\hat{\varepsilon}_i^{\tau}(t)$ where i is the satellite index, τ is the smoothing time, and t is time.

Smoothed code multipath statistics

For GPS L1-L5, the formula provided in [8] for the Airborne Accuracy Designator – Model A (AAD-A) [9] is given by:

$$\sigma_{n,user}^{GPS} = \sqrt{\frac{f_{L1}^4 + f_{L5}^4}{\left(f_{L1}^2 - f_{L5}^2\right)^2}} \sqrt{\left(\sigma_{MP}\right)^2 + \left(\sigma_{Noise}\right)^2} \tag{1}$$

$$\sigma_{MP}(\theta) = 0.13[\text{m}] + 0.53[\text{m}]\exp(-\theta/10[\text{deg}])$$

$$\sigma_{Noise}(\theta) = 0.15[\text{m}] + 0.43[\text{m}]\exp(-\theta/6.9[\text{deg}])$$

where θ is the elevation angle in degrees. The model used for GPS L1 is the same but without the dual frequency multiplying factor. We assumed the same model for Galileo E1-E5.

For each signal combination and each smoothing time τ, we form the normalized estimated error, that is:

$$\frac{\hat{\varepsilon}_i^{\tau}(t)}{\sigma_{i,user}^{GPS}}$$

and compare the resulting distribution to a unit gaussian. Only the measurements corresponding to a moving platform were kept (a thresholds of 50 m/s was used). After removing short arcs and removing the low speed data 34365 samples remained for the GPS L1-L5 iono free combination.

Figure 4 compares the quantiles of the normalized raw code multipath estimate (τ=1) to the quantiles of a unit gaussian for GPS L1-L5. As expected, the quantiles of the sample are above the unit gaussian (blue line) for positive values and below for negative values, which means that it is not an adequate bound. If we look at the results corresponding to 100 s smoothing (Figure 5), the quantiles of the sample are well within the quantiles of the unit gaussian, and therefore it is well bounded. The maximum ratio between the sample quantiles and the gaussian quantiles will provide the standard deviation of the minimum gaussian that bounds the sample distribution. In Figure 6 we show this ratio for all possible smoothing values between one and 100. When the line is below one, the error model is consistent with the observed errors.

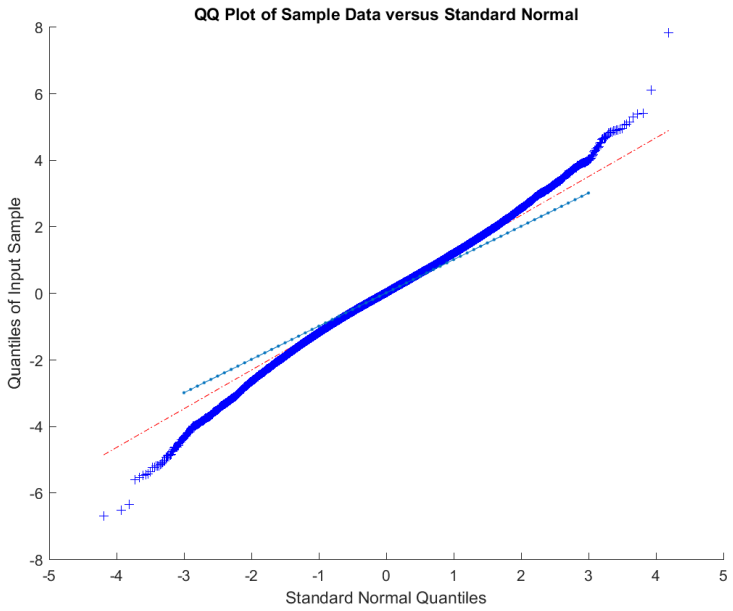

Figure 4. QQ plot of the estimate of the raw multipath normalized by the error model against a unit gaussian distribution for GPS L1-L5

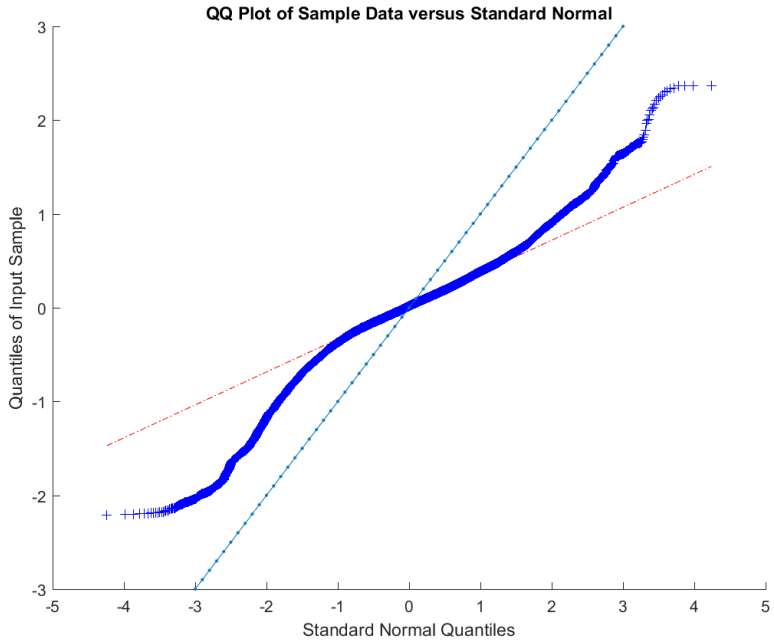

Figure 5. QQ plot of the estimate of the multipath noise after smoothing for a 100s normalized by the error model against a unit gaussian distribution for GPS L1-L5

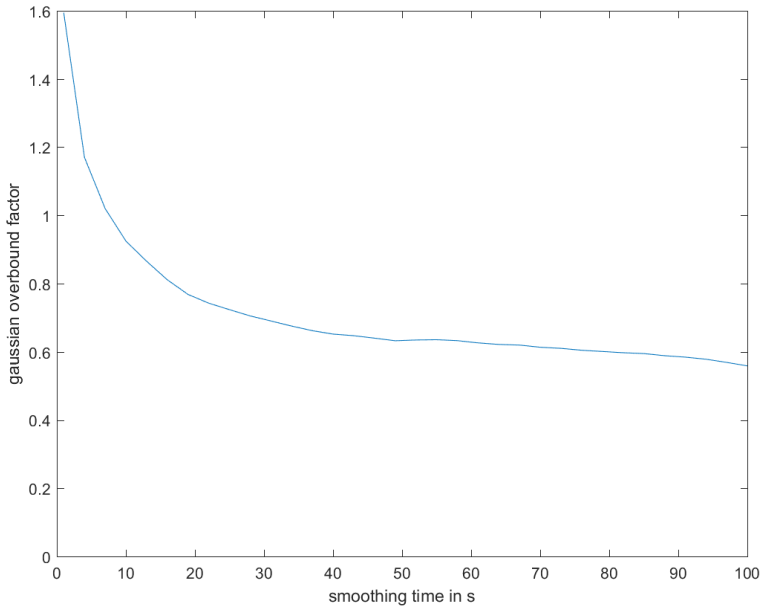

Figure 6. Multipath overbound estimate vs smoothing time (maximum ratio of sample quantile to unit gaussian quantile) for GPS L1-L5

Figure 7 shows the corresponding result for Galileo E1-E5. For these flight tests, the receiver was configured to track E5a and E5b, which is not entirely representative, as only E5a will be used in aviation receivers. There were 37412 samples. In this case, the bound almost works for the raw code. The value for a 100s is very close the one for GPS.

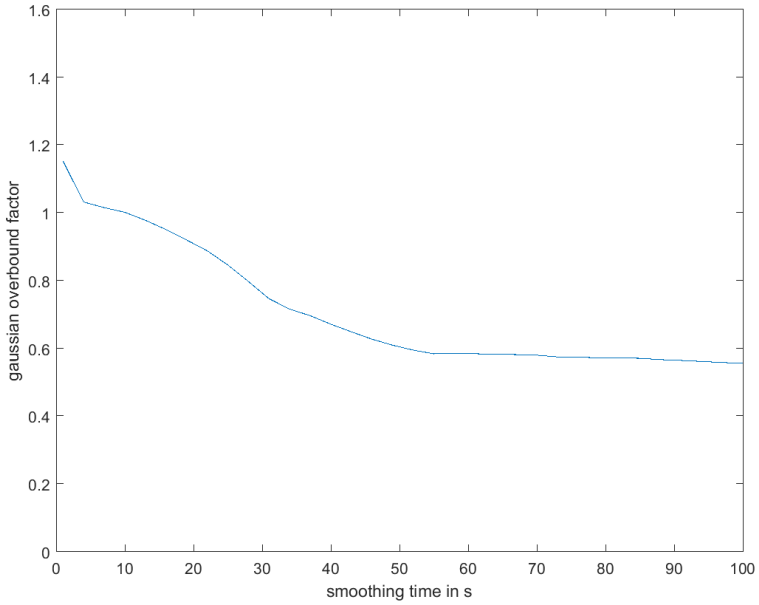

Figure 7. Multipath overbound estimate vs smoothing time (maximum ratio of sample quantile to unit gaussian quantile) for Galileo L1-L5

In order to account for the increased noise when the smoothing time is below 100 s, the multipath error bound in Equation (1) was inflated by the time dependent factor:

$$M(t) = \frac{\sqrt{\frac{1+\alpha}{t(1-\alpha)} - \frac{2\alpha}{t^2(1-\alpha)^2}\left(1-\alpha^t\right)}}{\sqrt{\frac{1+\alpha}{\tau(1-\alpha)} - \frac{2\alpha}{\tau^2(1-\alpha)^2}\left(1-\alpha^\tau\right)}}$$

Where:

t is the smoothing time

τ is smoothing constant (set to 100)

α is a parameter set to 0.84

This functional form was chosen because it corresponds to the variance of the smoothed code if we assume that the code multipath is a first order Markov process with correlation α. The value for α was chosen so that M(1)=3. This choice provides a curve that bounds the above results (Figures 6 and 7) with margin.

Elevation dependence

In this section we evaluate whether the error model captures the elevation dependence of the smoothed multipath errors. Figure 8 shows the smoothed code error normalized by the airborne multipath error model. As can be seen, the error model appears to account correctly for the elevation dependence for GPS. For Galileo, there seems to be a residual dependence left (although it could be due to sampling, as there are few samples).

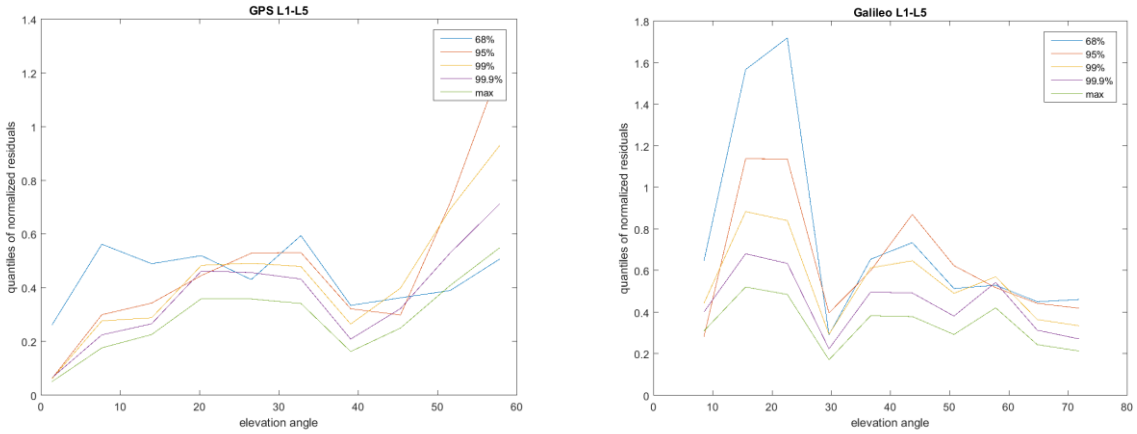

Figure 8. Quantiles of the normalized smoothed code multipath error divided by the corresponding unit gaussian quantile as a function of elevation angle for GPS L1-L5 (left) and for Galileo E1-E5 (right).

IMPACT OF AIRCRAFT BANKING

In this section, we show the effect of aircraft banking on the reception of the signals. Figure 9 shows the SNR for L1 and L5 for corresponding to the "figure eight" patterns (9 were flown). The repeated pattern can be clearly seen. There is a variation of more than 10 dB on from the highest SNR to the lowest, and it can reach 15 dB. The reduced power in L5 is due to the fact that the antenna is optimized for L1.

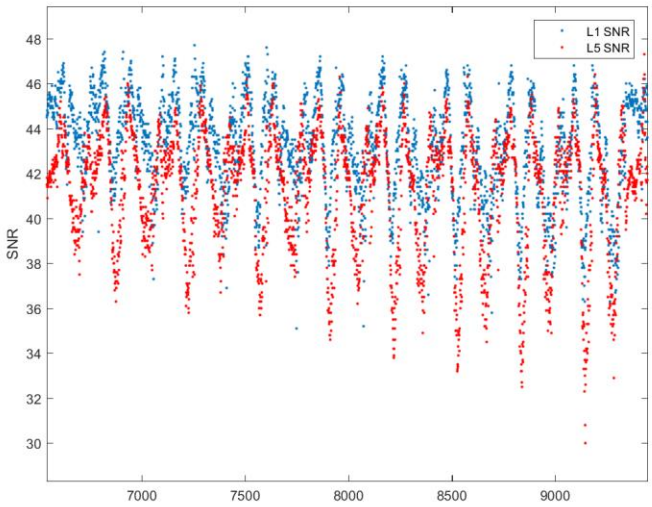

Figure 9. SNR for GPS L1 and L5 signals during the "figure eight" patterns.

Figure 10 shows the SNR for GPS L1 L2 semicodeless. The effect on L2 semicodeless is such that low elevation satellites are often lost as the aircraft banks (see results in [1]).

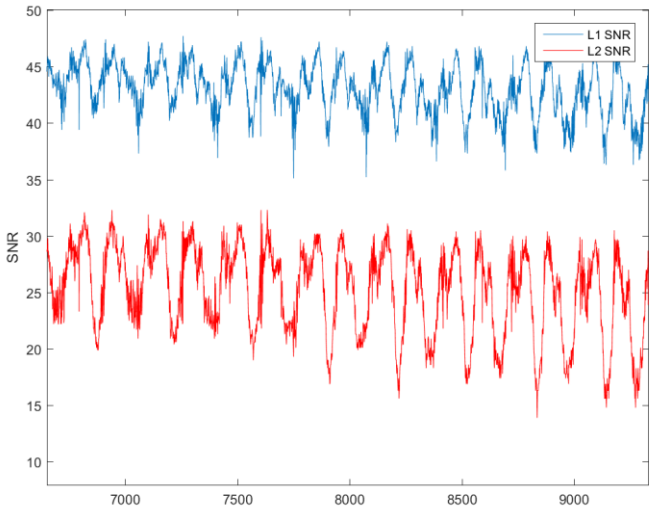

Figure 10. SNR for GPS L1 and L2 signals during the "figure eight" patterns.

This is not the case in L5, although we did see some instances. In Figure 1,1 we plot the elevation angle of the satellites in view as a function of time during the "figure eight" patterns. The loss of the lowest elevation satellite matches the pattern, as evidenced by the plot of the acceleration (the aircraft changes the bank angle side when the acceleration is close to zero). Assuming a coordinated turn, the bank angle was about 25 degrees.

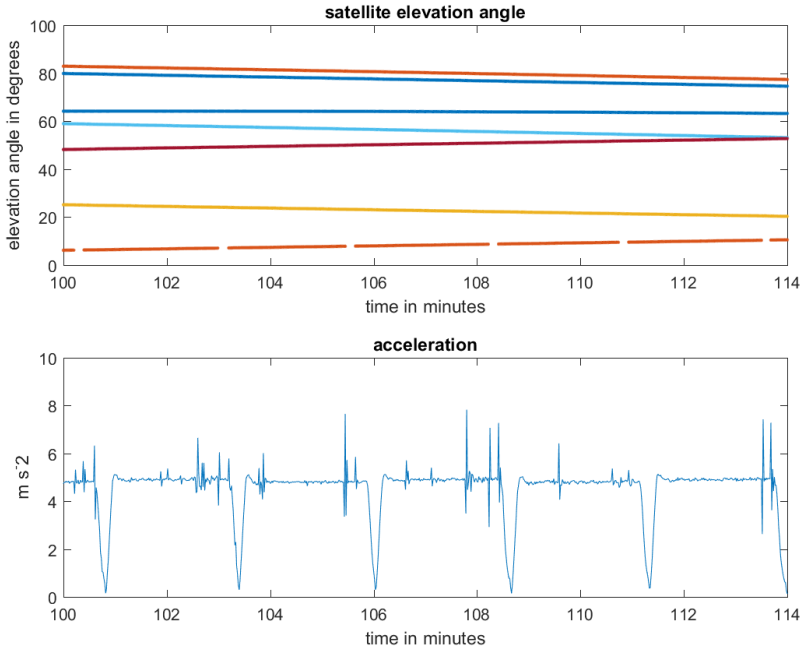

Figure 11. Satellite elevation angle and aircraft acceleration estimate

Figure 12 indicates the points where the satellite is lost (in red), the azimuth of the lost satellite, the shape of the aircraft, and the location of the antenna on the fuselage (red dot). It appears that the satellite is only lost when the line of sight is obstructed by the wings.

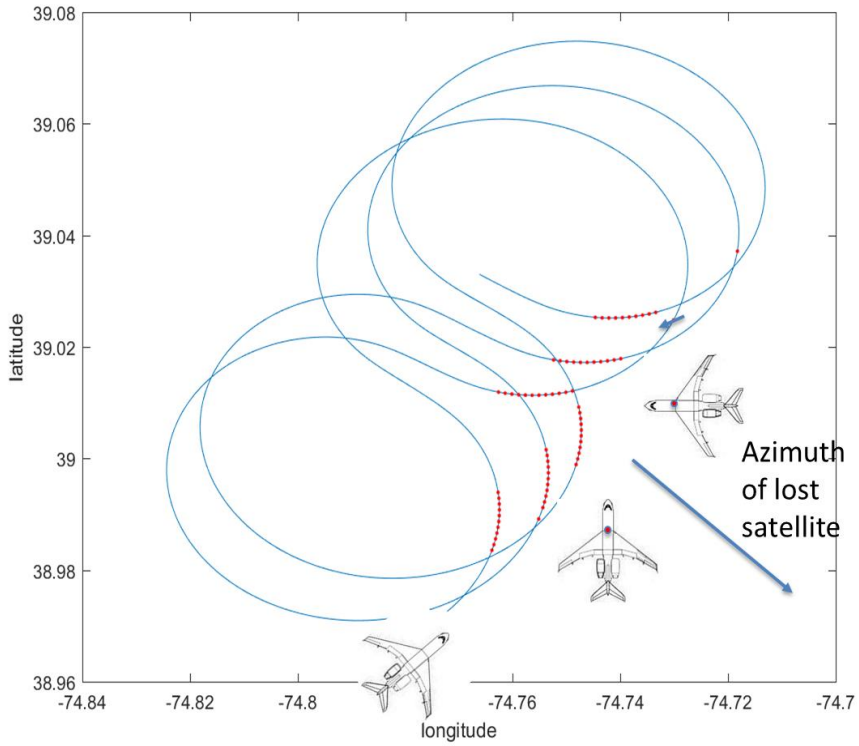

34

Figure 12. Figure eight patterns. The red section of the pattern shows where the satellite was lost.

ADVANCED RAIM AIRBORNE ALGORITHM RESULTS

In this section, we show the outputs of the ARAIM airborne algorithm described in [4] and [5] for L1 only and for L1-L5/E1-E5. For L1 only, we ran four different configurations: GPS, GPS-Galileo, GPS-GLONASS, GPS-Galileo-GLONASS. For L1-L5 we ran two different configurations GPS and GPS-Galileo. The Appendix shows additional results with GPS L1-L2 semicodeless and GPS L1-L2 semicodeless + GLONASS L1 L2.

Horizontal ARAIM: L1 only

ARAIM with L1 only would be intended for horizontal guidance [7]. The set of ARAIM parameters (which is included in the Integrity Support Message (ISM)) specified in Table 1 is representative of and ISM for horizontal guidance. In particular, a P_{sat} of 10^{-5} and a P_{const} of zero is assumed for GPS, which is what is effectively used in GPS RAIM now.

	GPS	Galileo	GLONASS
$Mask_i$	All 1	All 1	All 1
$P_{const,i}$	**0**	**10^{-4}**	**10^{-4}**

$P_{sat,j}$	**10^{-5}**	**10^{-4}**	**10^{-4}**
$\alpha_{URA,j}$	**1.0**	**1**	**1**
$\alpha_{URE,j}$	**1.0**	**1**	**1**
$b_{nom,j}$	**0.0**	**0.0**	**0.0**

Table 1. ISM settings for L1 (horizontal ARAIM)

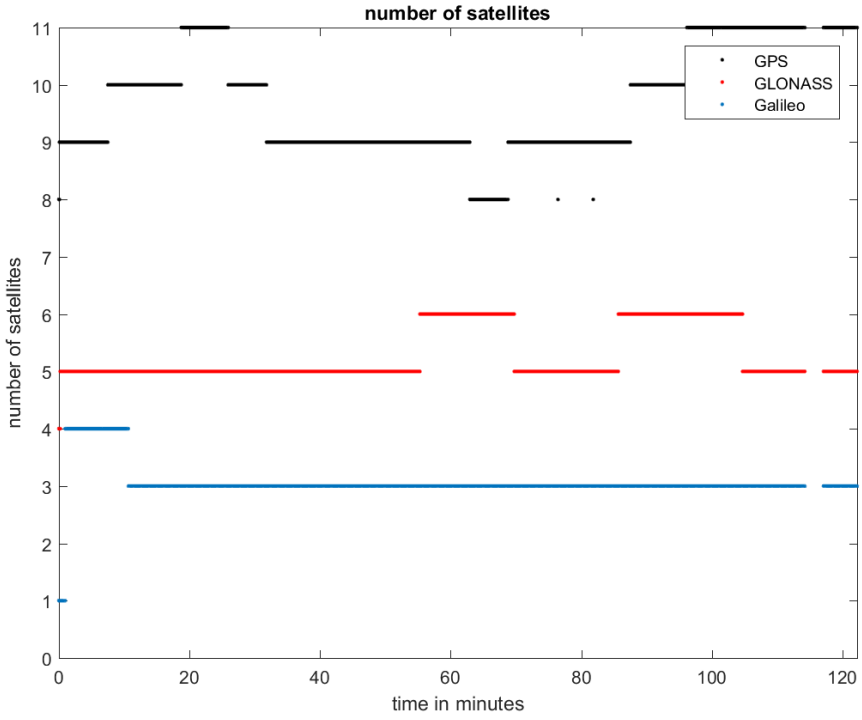

Figure 13. Number of satellites with L1/E1/G1 measurements

As can be seen in Figure 13 (the number of available measurements per constellation throughout the flight), GLONASS and Galileo are, as expected, much weaker than GPS. Figures 14 through 17 shows the Horizontal Protection Level (HPL) as computed by ARAIM for each of the constellation configurations for different elevation mask angles (5, 15, 25, and 30 degrees). These results illustrate how including a second and third constellation (even if weak) greatly improves the availability of ARAIM by maintaining low HPLs.

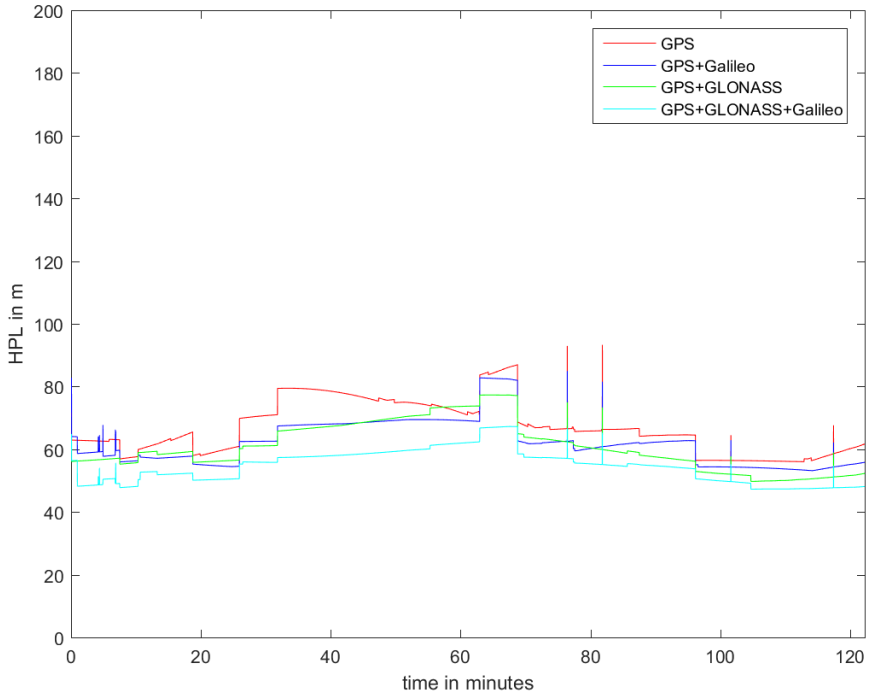

Figure 14. ARAIM L1 Horizontal Protection Levels for a 5 degree elevation mask angle

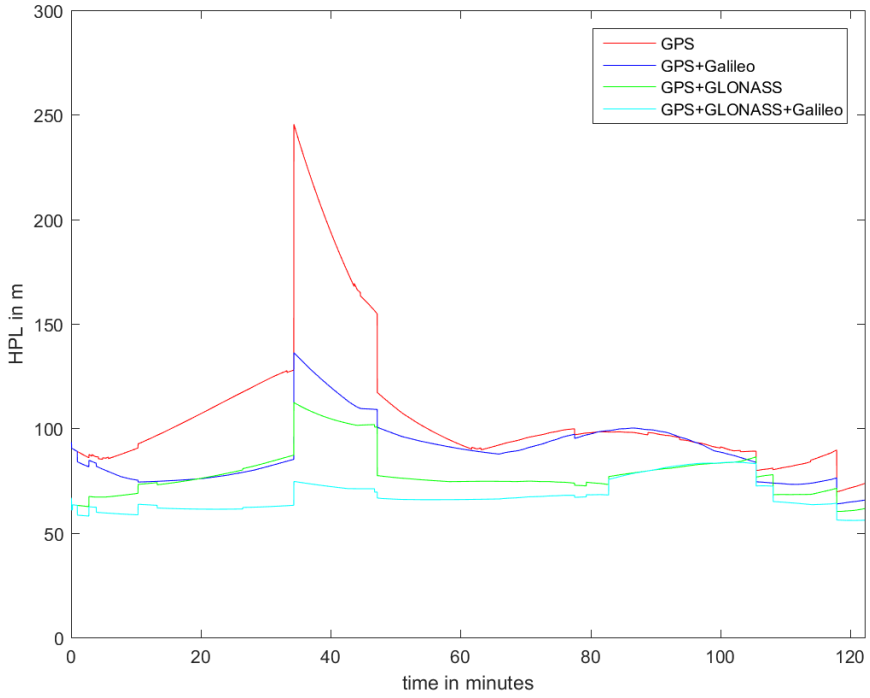

Figure 15. ARAIM L1 Horizontal Protection Levels for a 15 degree elevation mask angle

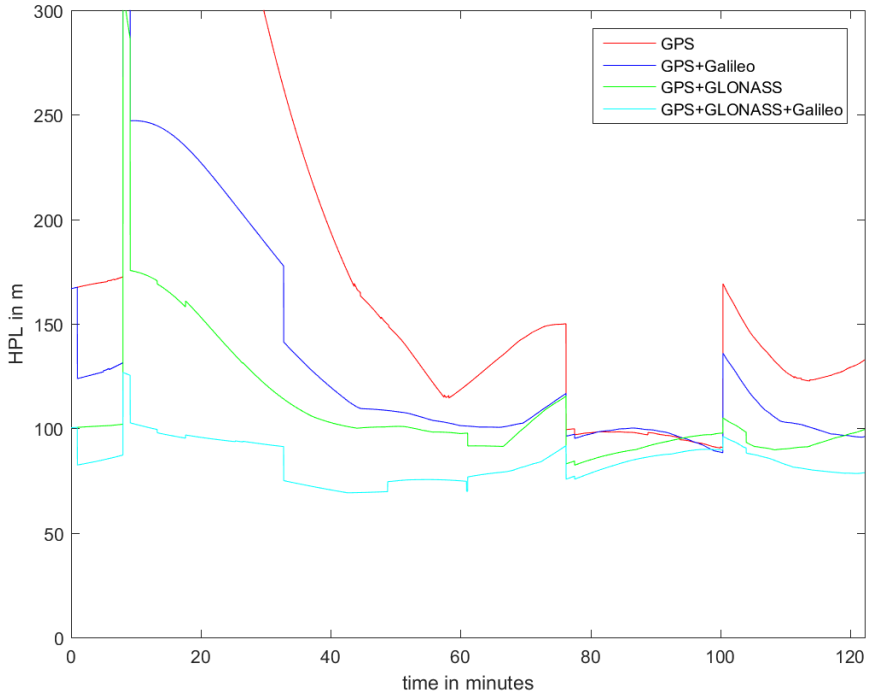

Figure 16. ARAIM L1 Horizontal Protection Levels for a 25 degree elevation mask angle

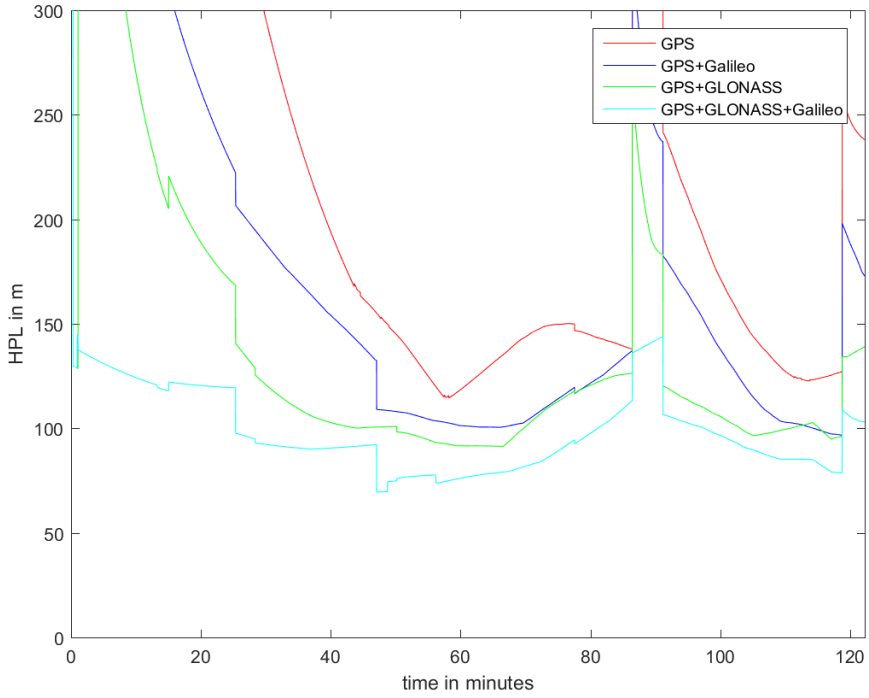

Figure 17. ARAIM L1 Horizontal Protection Levels for a 30 degree elevation mask angle

ARAIM with L1-L5

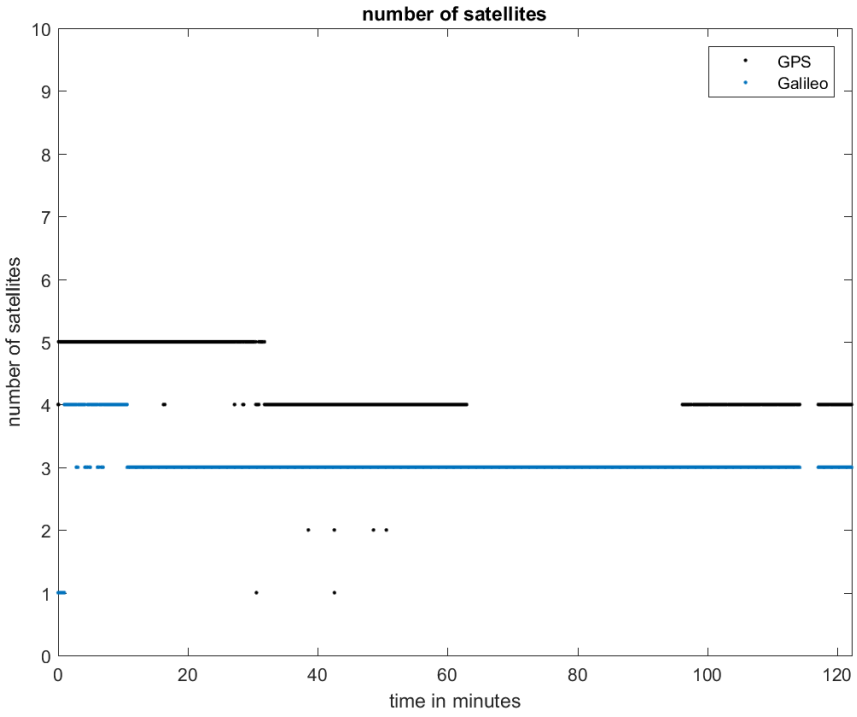

Figure 18. Number of satellites with L1-L5/E1-E5 measurements

Neither L5 in GPS nor Galileo had been declared operational when these measurements were taken (and therefore not subjected to a performance standard). Also, as shown in Figure 18, there are very few available measurements with both civil frequencies. The HPL results show in Figure 19 are therefore not surprising, as the HPL is directly impacted by the geometry. In addition, some of the L5 and E5 measurements suffered outages and cycle slips that caused the smoothing filter to re-start, and the nominal error bounds on the multipath to increase (following the curve specified above). The cause of these outages is not known, but it might be due to the lower SNR received in L5 (caused by the antenna).

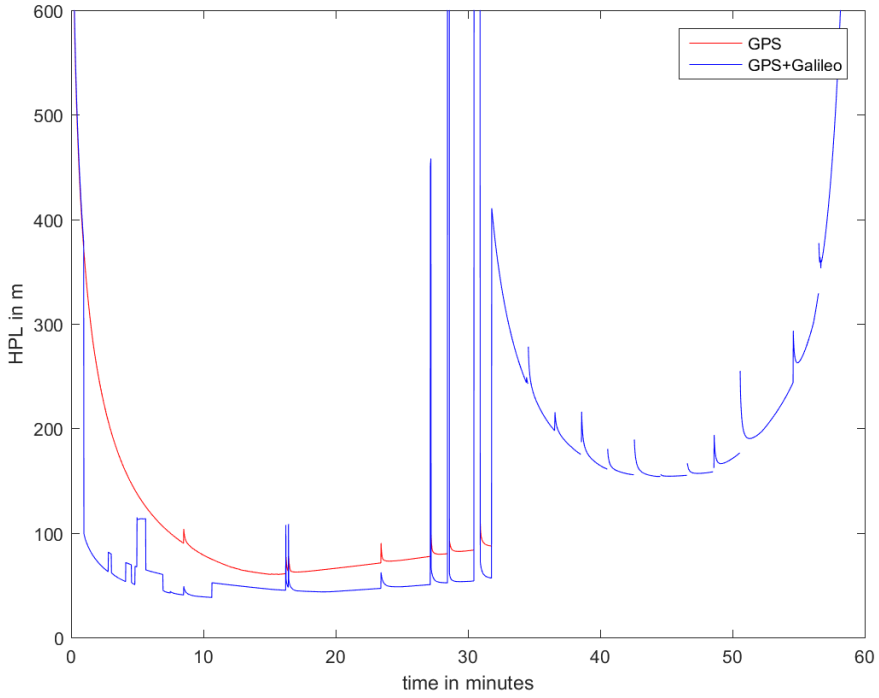

Figure 19. ARAIM L1-L5 Horizontal Protection Levels (5 degree elevation mask angle)

In the last set of results, we used an ISM representative for vertical guidance (Table 2). In this ISM, P_{const} for GPS is 10^{-4}, which requires the receiver to monitor constellation wide faults in GPS. For this reason, we can only hope to obtain finite PLs when both constellations have four or more available measurements, which only happens in the first ten minutes of the recorded data.

	GPS	Galileo
$Mask_i$	All 1	All 1
$P_{const,i}$	**0**	**10^{-4}**
$P_{sat,j}$	**10^{-5}**	**10^{-4}**
$\alpha_{URA,j}$	**1.0**	**1**
$\alpha_{URE,j}$	**1.0**	**1**
$b_{nom,j}$	**0.0**	**0.0**

Table 2. ISM settings for vertical guidance

Figure 20 shows the resulting Vertical Protection Levels (VPL). The gap between minute 5 and 7 is due to an exclusion event when the aircraft was static. This exclusion was due to a large multipath delay inconsistent with the error model (the error model is only needs to be valid in flight).

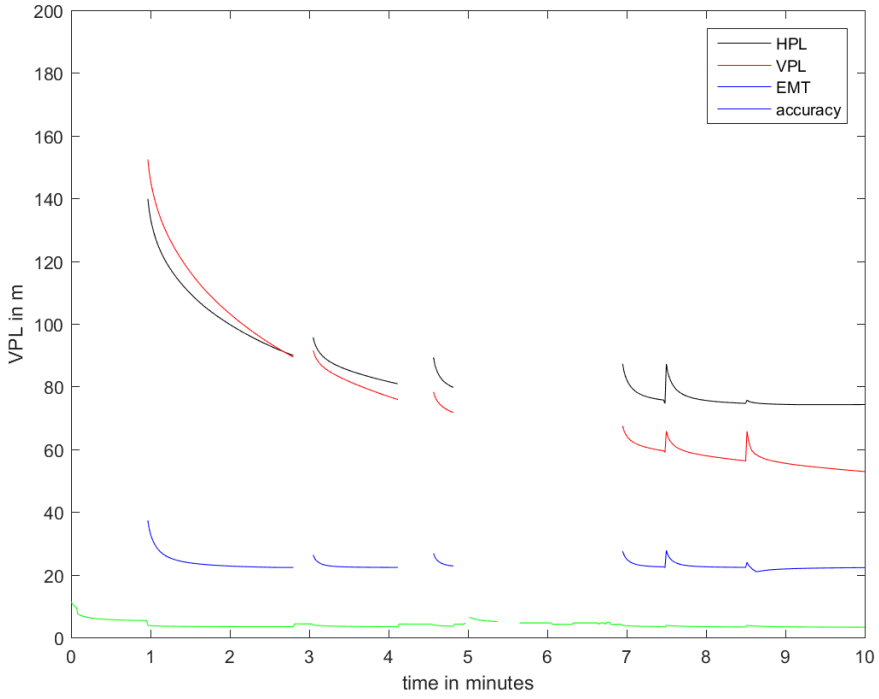

Figure 20. ARAIM L1-L5 Vertical Protection Level (5 degree elevation mask angle)

TEST STATISTICS

Here we provide a very preliminary view of the measurement statistics and how they compare with the error model. Since the error models are for flight conditions, we removed the data from epochs where the aircraft was static (a threshold of 50 m/s was used).

To this purpose, we collected the maximum normalized solution separation statistic for each epoch, which is written:

$$\max \frac{\left|\hat{x}_0 - \hat{x}_i\right|}{\sigma_{ss,i}}$$

Although the threshold against which it is computed is variable, it is always larger than 4.46 [5]. Figure 21 and 22 show the resulting histograms for the different L1 constellation configurations (corresponding to Figure 14), and for L1-l5 (corresponding to Figure 19). In both cases the test statistics are below one, although there is more margin in the L1 case (probably due to the use of the residual ionospheric delay bound, which is conservative in nominal conditions).

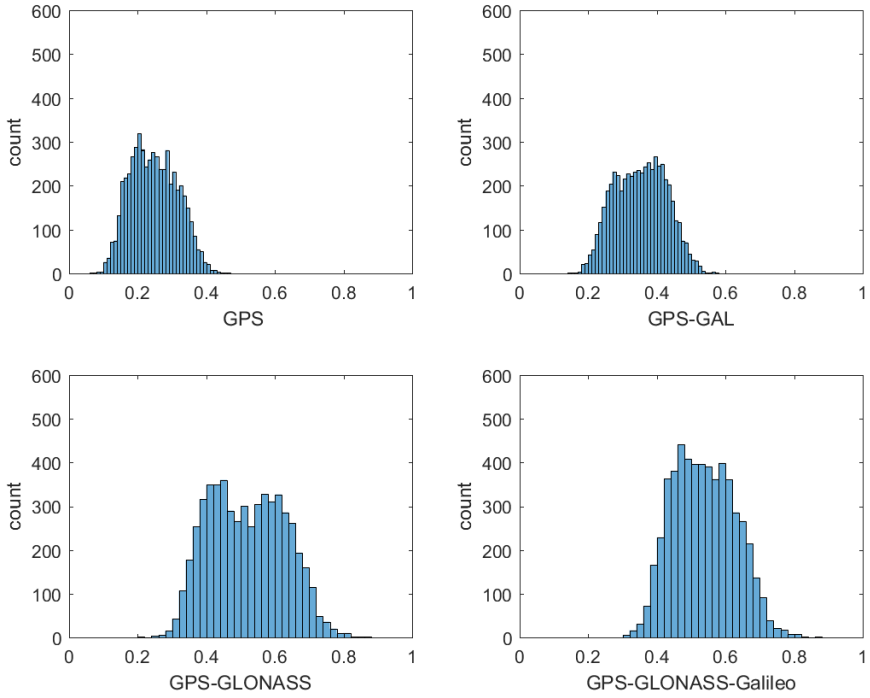

Figure 21. Histograms of maximum normalized solution separation statistics for L1 only

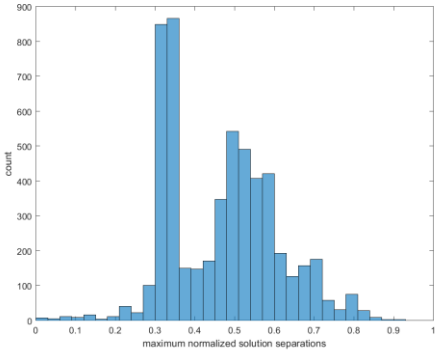

Figure 22. Histograms of maximum normalized solution separation statistics for L1-L5

Projecting errors in the parity space

In this work, we did not use a truth position. We can however assess the error model by projecting the measurements onto the parity space and examining the resulting residuals. Figure 23 shows the empirical cdf of the sum of the square of the measurement residuals normalized by the standard deviation of the pseudorange (which is the norm squared of the measurements projected onto the parity space). For comparison, we include the cdf of a chi-square statistic. We can see that, except at very low probabilities, the magnitude of the errors appears to be well bounded by the model. We do point out that this is only a sanity check, since we have very few data points.

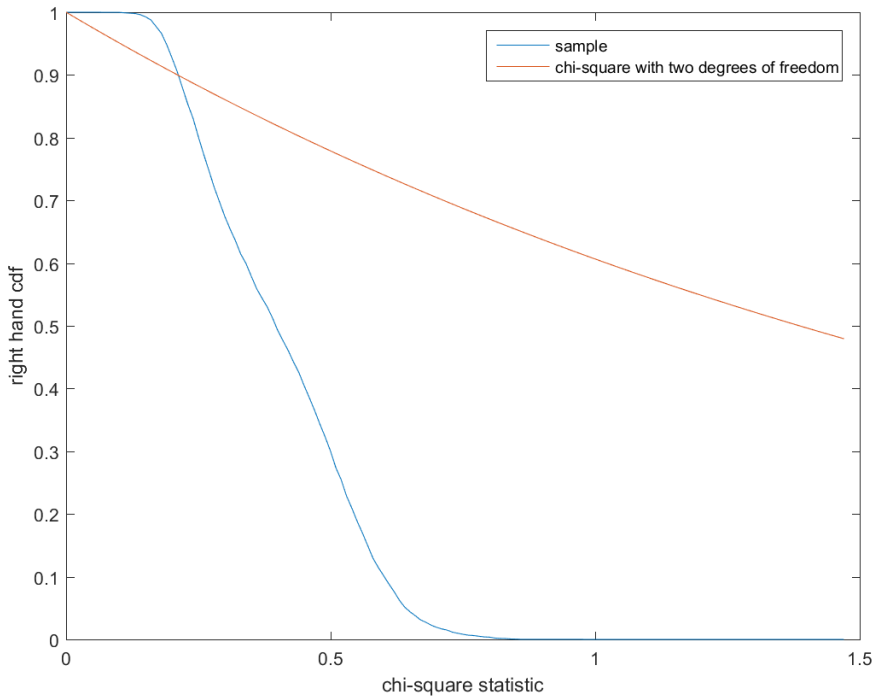

Figure 23. GPS-Galileo L1-L5 sum of squared residuals and comparison with chi-square cdf

SUMMARY

From a data set collected by an airborne receiver, we have characterized the multipath for different signal combinations. The error bound assumed in ARAIM simulations appears to be sufficiently conservative when the data has been smoothed for at least 100 s. For shorter smoothing times, or no smoothing, the multipath error can be larger. For this reason, we adjusted the error model as a function of time. An ARAIM airborne algorithm was applied to the data for two frequency combinations: L1 only and L1-L5. For L1 only (which is representative of Horizontal ARAIM), the results illustrate the benefits of including a second and third constellation (Galileo and GLONASS). Although, there are still few satellites with L5/E5 signals, we could still compute the ARAIM Protection Levels, even using the ISM parameters for vertical guidance. Finally, both for L1 and L1-L5, the collected data is consistent with the error models.

ACKNOWLEDGEMENTS

This work was funded by the Federal Aviation Administration. We would also like to thank Frank Lorge, Noah Rosen, and Bill Wanner at the FAA Technical Center (for making the data collection possible), and Stuart Riley at Trimble Navigation (for lending us the receiver and for his help in processing the data).

REFERENCES

[1] Phelts, R.E., Blanch, J., Chen, Y.-H., Riley, S., Enge,P. "ARAIM in flight using GPS and GLONASS," *Proceedings of the 29th International Technical Meeting of The Satellite Division of the Institute of Navigation (ION GNSS+ 2016)*, Portland, Oregon, September 2016

[2] Choi, M., Blanch, J., Walter, T., Akos, D., Enge, P., "Evaluation of Multi-constellation Advanced RAIM for Vertical Guidance Using GPS and GLONASS Signals with Multiple Faults," *Proceedings of the 25th International Technical Meeting of The Satellite Division of the Institute of Navigation (ION GNSS 2012)*, Nashville, TN, September 2012, pp. -.

[3] Choi, M., Blanch, J., Akos, D., Heng, L., Gao, G. Walter, T., and Enge, P., "Demonstration of Multi-Constellation Advanced RAIM for Vertical Guidance using GPS and GLONASS Signals," *Proceedings of the Institute of Navigation GNSS-11*, Portland, September 2011.

[4] Blanch, J., Walter, T., Enge, P., "A Simple Satellite Exclusion Algorithm for Advanced RAIM," *Proceedings of the 2016 International Technical Meeting of The Institute of Navigation*, Monterey, California, January 2016, pp. 239-244.

[5] Blanch, J., Walter, T., Enge, P., Lee, Y., Pervan, B., Rippl, M., Spletter, A., Kropp, V., "Baseline Advanced RAIM User Algorithm and Possible Improvements," *IEEE Transactions on Aerospace and Electronic Systems*, Volume 51, No. 1, January 2015.

[6] WAAS Minimum Operational Performance Specification (MOPS), RTCA document DO-229D.

[7] Working Group C, ARAIM Technical Subgroup, Milestone 3 Report, February 26, 2016. Available at: http://www.gps.gov/policy/cooperation/europe/2016/working-group-c/ http://ec.europa.eu/growth/tools-databases/newsroom/cf/itemdetail.cfm?item_id=8690

[8] RTCA/DO-208, "Minimum Operational Performance Standards for Airborne Supplemental Navigation Equipment Using Global Positioning System (GPS)," RTCA/DO-208, July 1991, prepared by RTCA Special Committee 159

[9] McGraw et. al, "Development of the LAAS Accuracy Models," *Proceedings of the ION GPS 2000*, Salt Lake City, UT

APPENDIX: ADDITIONAL MEASUREMENT STATISTICS

In this Appendix we include data that while not directly relevant to our goals, could be of interest in other applications.

Data availability

Except for very brief outages, L1 CA was almost always available whenever a GPS satellite was in view. This is also the case for GLONASS L1. In Tables A1 to A3 we show the availability of data relative to L1 for GPS, GLONASS and Galileo.

	L1 CA code	L2 C	L2 semi-codeless	L5
N. satellites	19	11	18	8

data avail. relative to L1 CA	100%	97.7%	94.3%	97.7%

Table A1. Data availability for GPS on 8/24/2016 flight test.

	L1 code	L2 semi-codeless
N. satellites	15	15
data avail. relative to L1	100%	89.7%

Table A2. Data availability for GLONASS on 8/24/2016 flight test.

	E1 code	E5
N. satellites	15	15
data avail. relative to L1	100%	99.2%

Table A3. Data availability for Galileo on 8/24/2016 flight test.

These tables and Figure A1 shows already that the availability of dual frequency measurements is not representative of what would be expected of a nominal system. Either there are too many lost measurements (case of L2 semicodeless), or there are not enough satellites (case of Galileo). This will directly impact the ARAIM outputs. We note that Galileo provides the strongest relative availability.

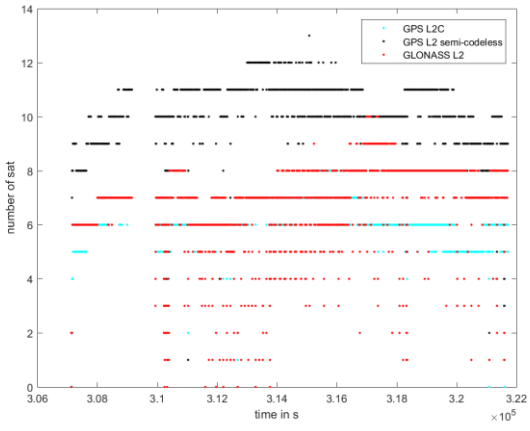

Figure A1. Number of measurements in view for L2.

Raw code multipath error distributions

From the results of the carrier leveling process (the black curve in Figures 2 and 3) we can characterize the statistics of the dual frequency code multipath. Figure 4 shows the raw error distribution for GPS L1-L5 (58873 samples). Although the core seems well behaved, this empirical distribution contains outliers as large as 22.4 m.

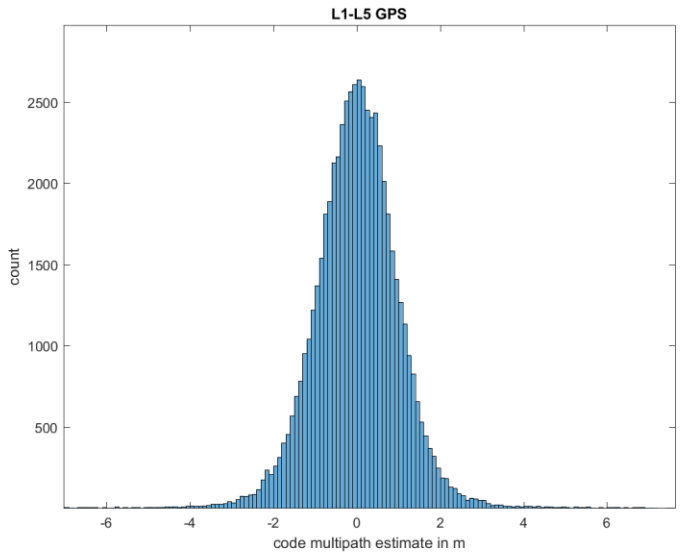

Figure A2. Code multipath estimate for GPS L1-L5 iono free combination.

Table A4 gives a summary of the raw distribution for each of the signals. Each of the entries corresponds to the quantile of the corresponding histogram. One can see that, in this data set, the multipath is roughly twice as large as in GPS, which is what is expected from the difference in chipping rate. We also remark that the multipath in the Galileo signals is much smaller (the receiver was using both E5a and E5b, which is not representative of an aviation receiver, where only E5a will be used).

	GPS L1 –L5	GPS L1 – L2C	GPS L1 –L2 semicodeless	GLONASS L1 – L2	Galileo L1 –L5
Standard deviation	1.1 m	1.3 m	1.1 m	2.2 m	0.7 m
68%	0.9 m	1.0 m	1.0 m	1.6 m	0.6 m
95%	2.0 m	2.2 m	2.1 m	3.4 m	1.3 m
99%	3.3 m	3.6 m	3.2 m	5.2 m	2.2 m
99.9%	8.0 m	10.2 m	6.5 m	18.9 m	3.7 m
99.99%	13.5 m	18.2 m	13.1 m	59.6 m	6.4 m
maximum	22.4 m	29.1 m	27. 4 m	72.1 m	6.5 m

Table A4. Quantiles of the multipath estimates for each dual frequency combination

Elevation dependence

Figures A3 through A6 show how the statistics of the code multipath depend on the elevation angle. This dependence is particularly strong for low elevation angles in GLONASS.

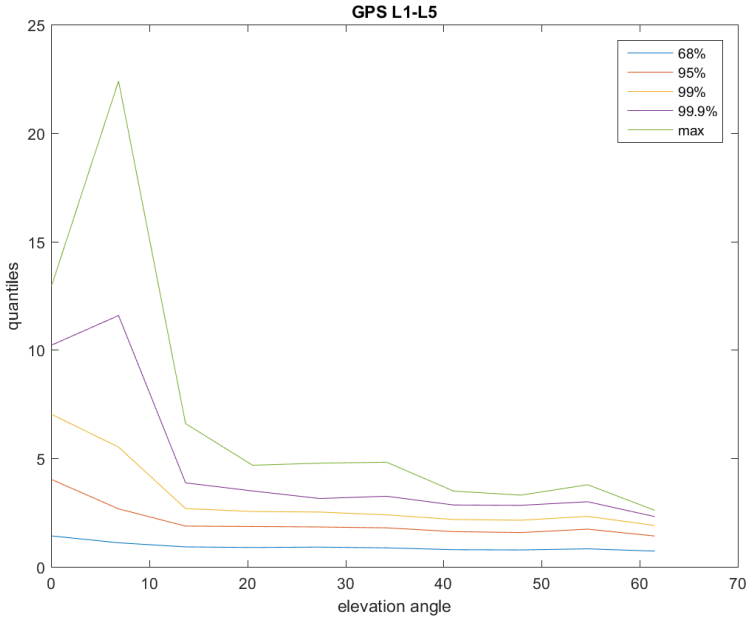

Figure A3. Code multipath statistics as a function of elevation angle for GPS L1-L5

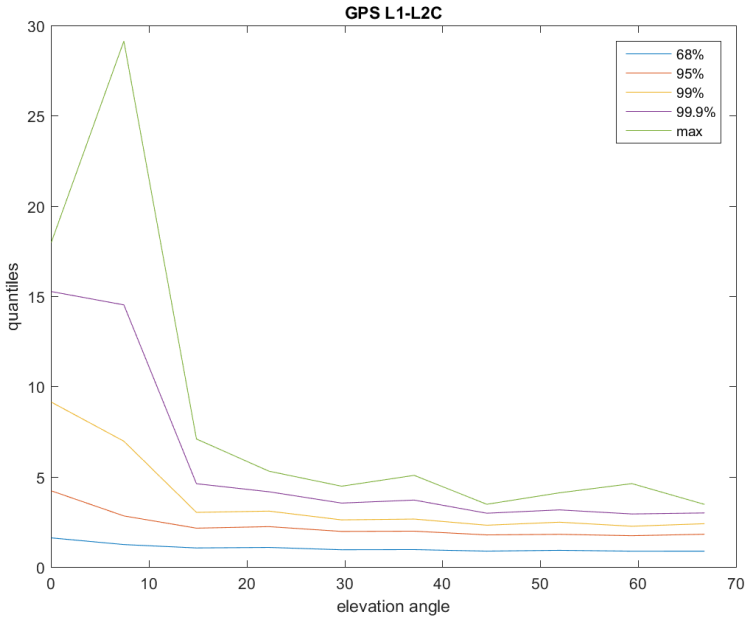

Figure A4. Code multipath statistics as a function of elevation angle for GPS L1-L2C

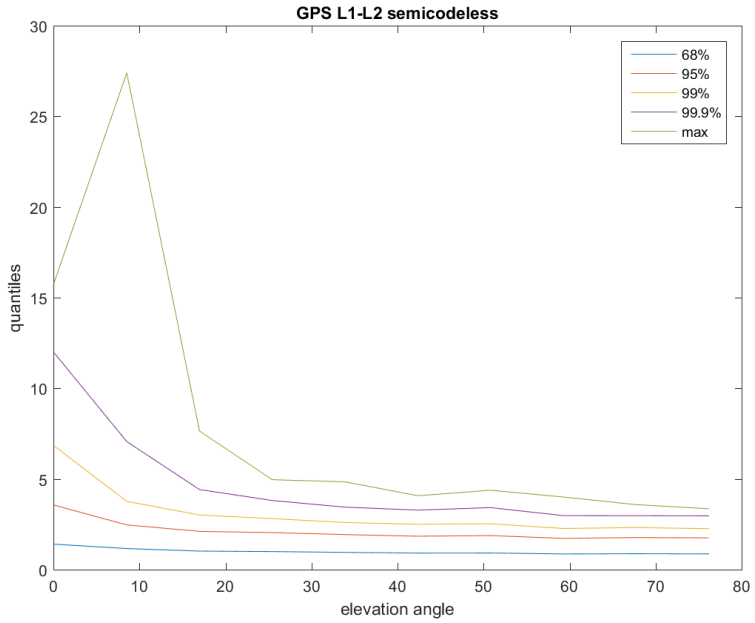

Figure A5. Code multipath statistics as a function of elevation angle for GPS L1-L2 semicodeless

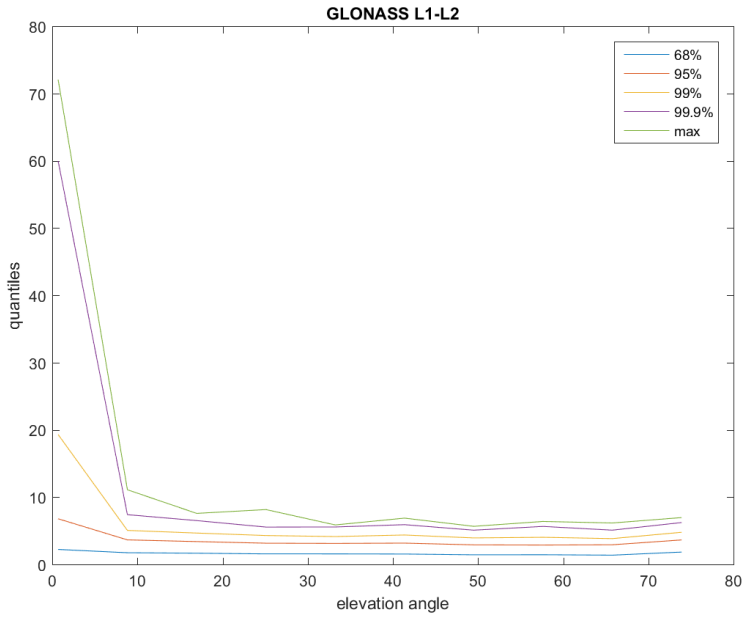

Figure A6. Code multipath statistics as a function of elevation angle for GLONASS L1-L2 semicodeless

Signal to noise (SNR) ratio dependence

The dependence on SNR (which was taken to be the minimum of the two signals) appears to be much weaker than the elevation angle dependence, as can be seen in Figures A7 to A9.

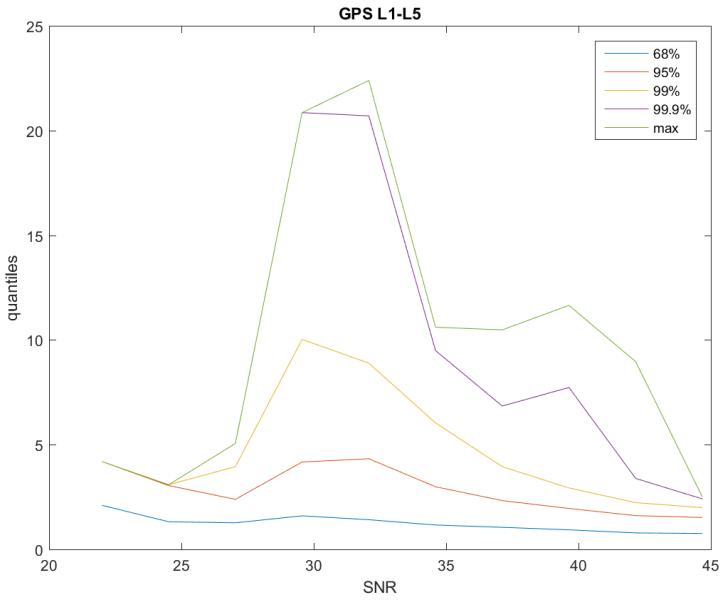

Figure A7. Code multipath statistics as a function of SNR for GPS L1-L5

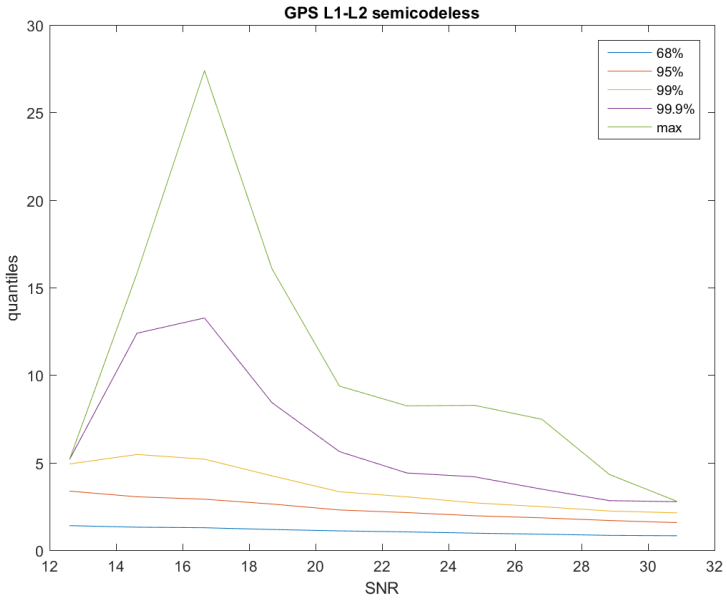

Figure A8. Code multipath statistics as a function of SNR for GPS L1-L2 semicodeless

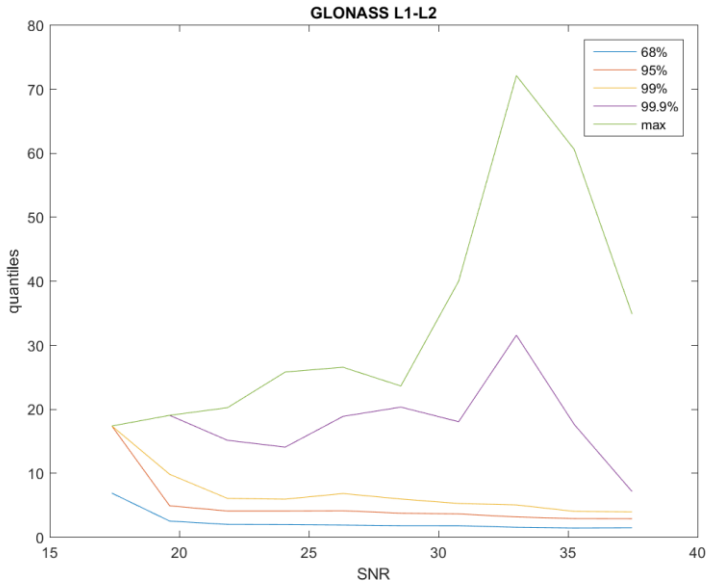

Figure A9. Code multipath statistics as a function of SNR for GLONASS L1-L2 semicodeless.

Temporal correlation

We now examine the temporal correlation of the code multipath. As can be seen in Figure A10, it takes the decorrelation constant is on the order of 15 s (that is, it takes about 15 s for the decorrelation to reach 1/e). However, the decorrelation does not appear to be exponential: after an initial large decorrelation after one sample (to 0.5), the decorrelation slows down.

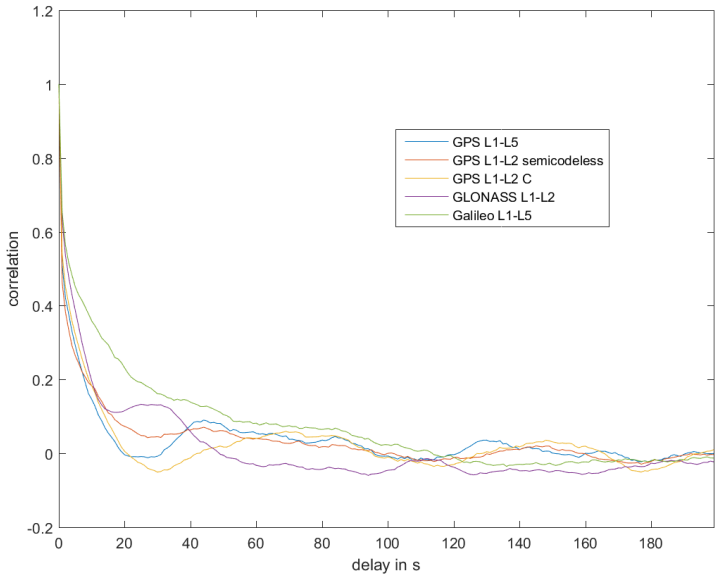

Figure A10. Temporal correlation of code multipath

Statistics of carrier smoothed multipath error normalized by error model

Table A5 provides a set of metrics on the statistics of the normalized residuals for each combination. Each entry corresponds to the containment of the sample distribution for a given percentile divided by the corresponding unit gaussian containment. If the sample distribution were exactly gaussian, then all entries would be one; if the sample distribution has a smaller containment, the ratio is smaller than one. As can be seen, the model appears to be sufficiently conservative.

	GPS L1 –L5	Galileo E1-E5	GPS L1 – L2C	GPS L1 –L2 semicodeless	GLONASS L1 – L2
Standard deviation	0.5		0.5	0.5	0.7
68%	0.2		0.2	0.2	0.3
95%	0.7		0.7	0.8	1.1
99%	1.1		1.4	1.4	1.9
99.9%	1.7		1.9	2.1	3.3
99.99%	2.3		2.5	2.5	3.8
maximum	2.4		2.6	2.9	3.8

TableA 5. Quantiles of the normalized smoothed code multipath error

ARAIM with GPS L1-L2 semicodeless

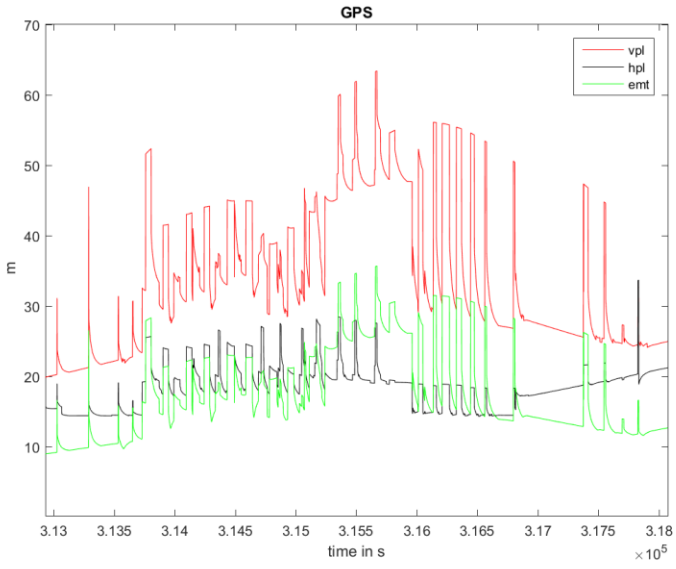

Figure A11. ARAIM outputs for GPS L1-L2 semicodeless. The peaks are due to the loss of L2 semicodeless.

In this case, there were no exclusions. The histogram of the solution separation statistics is shown in Figure A11. It is compatible with the assumed error model.

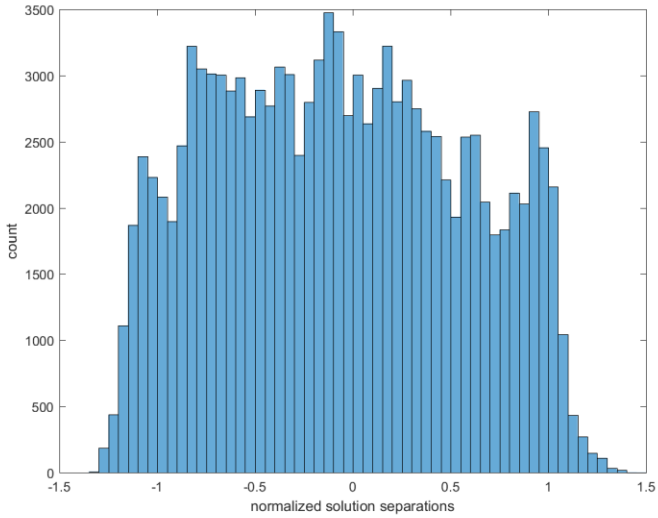

Figure A12. Histogram of normalized solution statistics.

GPS L1-L2 semicodeless - GLONASS

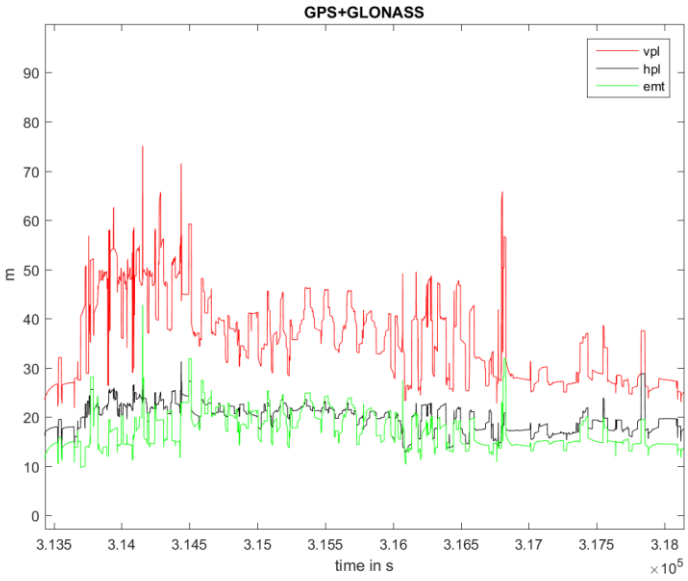

Figure A13. ARAIM outputs for GPS GLONASS L1-L2 semicodeless. The peaks are due to the loss of L2 semicodeless.